Supplemental Information: Remotely sensing river greenhouse gas exchange velocity using the SWOT satellite

Craig B Brinkerhoff[1,✉], Colin J Gleason[1], Christopher J Zappa[2], Peter A Raymond[3], and Merritt E Harlan[1]

[1] Department of Civil & Environmental Engineering, University of Massachusetts, Amherst, MA
[2] Lamont-Doherty Earth Observatory, Columbia University, Palisades, NY
[3] School of the Environment, Yale University, New Haven, CT

✉ Correspondence: Craig B Brinkerhoff <cbrinkerhoff@umass.edu>

Contents

This supplementary information contains 6 texts, 6 figures and 4 tables.

Test S1: Estimating how hydraulically wide SWOT rivers are

To quantify the prevalence of hydraulically-wide, SWOT-observable rivers, we used the dataset of field-measured river hydraulics outlined in Section 2.1. That dataset has over 500,000 discrete measurements of river width, velocity, area, and discharge that were made by the United States Geological Survey (USGS) to calibrate streamgauge rating curves. Here, we describe how this dataset was filtered down to 22452 SWOT-observable rivers.

First, we removed all measurements tagged by the USGS as 'poor', measurements with non-finite values, or measurements of 0. While this would indicate a dry channel, our hydraulic geometry model necessitates within-bank flow. Likewise, because hydraulic geometry only applies to within-bank flows and not flood events, we remove all overbank flows. This was done by first filtering for sites with at least 20 measurements (to build robust estimates of bankfull hydraulics) and then calculating bankfull width and depth as the width or depth with a return period of two years. While the only true way to calculate bankfull hydraulics is manually in the field, this is obviously impractical here. A two-year return period is a standard approximation for determining out-of-bank flow in single-channel meandering rivers and was the method used by Brinkerhoff et al. (2019). We then removed all measurements with a width or depth beyond their respective at-a-station 2 year values.

Finally, we filtered this dataset to only measurements at least 100m wide ('SWOT-observable'). This left us with 22452 total river hydraulics measurements.

Text S2: Gas exchange model derivations

In this text we provide the full algebra to arrive at the four physically-based gas exchange models we tested in this study. Consult Appendix A for all variable definitions. Subscripts denote variants of the same parameter, depending on which ϵ model is employed (see Main Text).

Small-eddy models (Equation 3 from Main Test)

Log-law-of-the-wall model for the turbulent dissipation rate (assume $\epsilon = \epsilon_S$)

$$k_{600} = \beta_1(\epsilon_S)^{1/4} \quad (\mathbf{S1})$$

$$k_{600} = \beta_1\left(\frac{U_*^3}{H}\right)^{1/4} \quad (\mathbf{S2})$$

$$k_{600} = \beta_1\left(\frac{\sqrt{gR_h}S^3}{H}\right)^{1/4} \quad (\mathbf{S3})$$

$$k_{600} = \beta_1\left(\frac{(gHS)^{3/2}}{H}\right)^{1/4} \quad (\mathbf{S4})$$

$$log(k_{600}) = \beta_1 + \frac{3}{8}log(gS) + \frac{1}{8}log(H) \quad (\mathbf{S5})$$

Form-drag model for the turbulent dissipation rate (assume $\epsilon = \epsilon_D$)

$$k_{600} = \beta_1(\epsilon_D)^{1/4} \quad (\mathbf{S6})$$

$$log(k_{600}) = \beta_1 + \frac{1}{4}log(gS\bar{U}) \quad (\mathbf{S7})$$

Reynolds extension models (Equation 4 from Main Text)

Log-law-of-the-wall model for the turbulent dissipation rate (assume $\epsilon = \epsilon_S$)

$$k_{600} = \beta_1 (\epsilon_S)^{1/4} A_p^{3/4} \textbf{(S8)}$$

$$k_{600} = \beta_1 \left(\frac{U_*^3}{H}\right)^{1/4} \left((U_* H)^{1/2}\right)^{3/4} \textbf{(S9)}$$

$$k_{600} = \beta_1 U_*^{9/8} H^{1/8} \textbf{(S10)}$$

$$k_{600} = \beta_1 (g R_h S)^{9/16} H^{1/8} \textbf{(S11)}$$

$$k_{600} = \beta (g H S)^{9/16} H^{1/8} \textbf{(S12)}$$

$$log(k_{600}) = \beta_1 + \frac{9}{16} log(gS) + \frac{11}{16} log(H) \textbf{(S13)}$$

Form-drag model for the turbulent dissipation rate (assume $\epsilon = \epsilon_D$)

$$k_{600} = \beta_1 (\epsilon_D)^{1/4} A_p^{3/4} \textbf{(S14)}$$

$$k_{600} = \beta_1 (g S \bar{U})^{1/4} \left((U_* H)^{1/2}\right)^{3/4} \textbf{(S15)}$$

$$k_{600} = \beta_1 (g S \bar{U})^{1/4} (g R_h S)^{3/16} H^{3/8} \textbf{(S16)}$$

$$k_{600} = \beta_1 (g S \bar{U})^{1/4} (g H S)^{3/16} H^{3/8} \textbf{(S17)}$$

$$log(k_{600}) = \beta_1 + \frac{7}{16} log(gS) + \frac{1}{4} log(\bar{U}) + \frac{9}{16} log(H) \textbf{(S18)}$$

Text S3: Bayesian linear regression hyperparameterization

As detailed in section 2.4, we fit a Bayesian linear regression model using equation 7 and our 166 estimates of hydraulically-wide k_{600} Here, we provide the model specification. Equation S19 is the regression equation and the prior hyperparameterizations are equations S20-S24. Priors are specified as normal distributions $N(\mu, \sigma^2)$, save σ_{LM} which is characteristically specified as an exponential distribution.

$$log(k_{600}) = \beta_1 + \alpha_1 log(gS) + \alpha_2 log(\bar{U}) + \alpha_3 log(H) \textbf{(S19)}$$

$$\alpha_1 \sim N\left(\frac{7}{16}, \frac{1}{8}^2\right) \textbf{(S20)}$$

$$\alpha_2 \sim N\left(\frac{1}{4}, \frac{1}{8}^2\right) \textbf{(S21)}$$

$$\alpha_3 \sim N\left(\frac{9}{16}, \frac{1}{8}^2\right) \textbf{(S22)}$$

$$\beta_1 \sim N(0, 1^2) \textbf{(S23)}$$

$$\sigma_{LM} \sim exp(1) \textbf{(S24)}$$

The equation 7 coefficients, derived from geomorphic assumptions of the SWOT-observable river channel, were used to assign reasonably informative priors for α_1, α_2, and α_3. For the other models in Figure S1, the prior distribution means for α_1, α_2, and α_3 were changed to their respective coefficients derived in Text S2. β_1 and the model uncertainty σ_{LM} were left as uninformative given that we lack any prior knowledge of what they might be.

Text S4: BIKER hyperparameterization

In this text we explain in detail how BIKER's prior distributions were determined for a given river.

Prior distributions are defined by their hyperparameters. For BIKER, prior distributions are formalized as truncated normal distributions of the log-transformed terms such that $log(X) \sim \mathcal{N}(\mu, \sigma^2)$ for $\lambda < log(X) < \gamma$, using prior hyperparameters mean (μ), standard deviation (σ), and upper (γ) and lower bounds (λ) for any parameter X. It is important to again stress, as we do in the Main Text, that BIKER prior hyperparameters are described using only SWOT data to be completely globally implementable. This use of the data to describe the priors is analogous to the 'empirical Bayes method' (Hoff, 2009).

A_{0_i} and n_i prior hyperparameters were assigned following Brinkerhoff et al. (2020). They developed a set of river channel prior hyperparameters for McFLI algorithms that are entirely RS-able and reflect differential channel hydraulics as a function of river geomorphology. They used an extensive database of field measurements and statistical learning to identify patterns that associate river width with the hydraulic priors needed to run McFLIs so that prior hyperparameters are assigned to rivers using only the remotely sensed measurements. For this study, we extracted A_{0_λ} and A_{0_γ} as the 5th and 95th percentile values rather than the absolute maximum and minimum values to avoid physically impossible bounds on A_0.

This leaves the k_{600_t} hyperparameters to be defined. k_{600_μ} is set by invoking the hydraulic geometry (HG) relationships described in Section 3.2.3 of the main text and Table S3 using the

data from Brinkerhoff et al. (2019). We replaced both depth and velocity terms from our gas exchange model (Equation 7 in the Main Text) with these HG models, resulting in Equation S25 where Q is the mass-conserved streamflow for the river reach.

$$k_{600_\mu} = 62.82\left(gS_{i,t}\right)^{7/16}(0.252Q^{0.388})^{9/16} * (0.276Q^{0.164})^{1/4} \quad \mathbf{(S25)}$$

Obviously, we have no a priori information about Q. So, we use the Q prior that will be globally available when SWOT launches: a mean annual estimate from a water balance model. This is the standard prior information used to benchmark the SWOT discharge algorithms and is provided with the simulated SWOT data by both Durand et al. (2016) and Frasson et al. (2021). Using a temporally-invariant estimate of streamflow is the worst case scenario and BIKER's performance will improve with a more informed prior on streamflow (and therefore k_{600}). However as noted in the Main Text, our primary goal with this initial validation is to benchmark BIKER's worst case scenario for performance and so we do that here.

k_{600_σ} is set to 0.58 (log-space). This was provided by posterior mean σ_{LM} from the Bayesian linear regression (equation 8 and Table 1) in the main text (Text S3 as well). k_{600_λ} was set to log(0.001) m/day. k_{600_γ} was set to log(500) m/day.

Text S5: Determining complete BIKER model uncertainty

Recall that $\sigma_{k_{600}}$ refers to the total uncertainty inherent in Equation 10, i.e. stemming from the Reynolds-extension model (Equation 8) and Manning's equation for $\bar{U}$. For the purposes of this study, we are validating BIKER against Equation 8 in the main text and so all uncertainties associated with the β_1 parameter are ignored and we only need to reflect the Manning's uncertainty in our specification of $\sigma_{k_{600}}^2$. Therefore, we take Hagemann et al. (2017)'s estimated uncertainty from Manning's equation to infer streamflow from SWOT observations (0.25) and inflate it slightly to also account for the hydraulically-wide channel assumption and arrive at 0.30. This is the $\sigma_{k_{600}}$ used in this study.

In the scenario that BIKER is run on real SWOT data, $\sigma_{k_{600}}$ must reflect the full uncertainty implicit in Equations 10 and 11 in the main text. This means we must also account for uncertainty from the β_1 parameter. Assuming perfect, no-error measurements are made by the SWOT satellite, the full Equation 8 uncertainty is expressed for some set of hydraulic observations as Equation S25. To quantify total uncertainty in k_{600}, we push Monte Carlo simulations through Equation S25 and take the mean uncertainty as a reasonable value for $\sigma_{k_{600}}$ once SWOT launches.

More specifically, we use the 166 hydraulically-wide measurements in our field-measured k_{600} dataset (Section 2 in the Main Text) and run 166 different Monte Carlo simulations using the distributions for α_1, α_2, α_3, β_1, k_{600_σ}, and the Manning's equation uncertainty (0.30 in log-space). Note that each Monte Carlo simulation is itself 10,000 runs in order to obtain a distribution of k_{600} estimates. For each of the 166 distributions of estimated k_{600}, we extract the standard deviation as

the uncertainty. We then take the average of those standard deviations to be a reasonable estimate of $\sigma_{k_{600}}$. This ultimately provided a value of 0.71 and should be used when running BIKER on real SWOT data.

Text S6: Literature $[CO_2]$ flux models

Here, we describe in more detail the three $[CO_2]$ flux models used to compare against BIKER in Section 3.2.3. The specific equations used are outlined in Table S3.

In brief, gas fluxes ($[FCO_2]$) are only obtainable at the global scale via predictive equations for k_{CO_2} per Equation 2 and 13. Here, we obtain $[FCO_2]$ using the in situ $[CO_2]$ data described in Section 3.1 and k_{CO_2} estimates. The k_{CO_2} estimates are calculated using Equation 8. Equation 8 is calculated using 1) in situ streamflow data, and 2) hydraulic scaling equations from the literature that predict river velocity and depth from streamflow. Specifically, these literature equations are the 'Raymond 2012', 'Raymond 2013', and 'Brinkerhoff 2019' models (Table S3).

For example, the 'Raymond 2012' model uses the hydraulic scaling equations from Raymond et al. (2012) to predict velocity and depth, which are in turn used to calculate a k_{CO_2} via equation 8, which finally is used to calculate $[FCO_2]$ via equation 1. Similarly, the 'Raymond 2013' model uses the equations outlined in Raymond et al. (2013) and the 'Brinkerhoff 2019' model uses new equations fit to the hydraulics dataset from Brinkerhoff et al. (2019) after the filtering described in Text S1. We chose to include the 'Brinkerhoff 2019' model as the training dataset is far larger than those used in either of the previous two models (Table S3: 104,624 versus 10,837 versus 1,026, respectively). Finally, we converted from k_{600} to k_{CO_2} following Raymond et al. (2012).

Figure S1

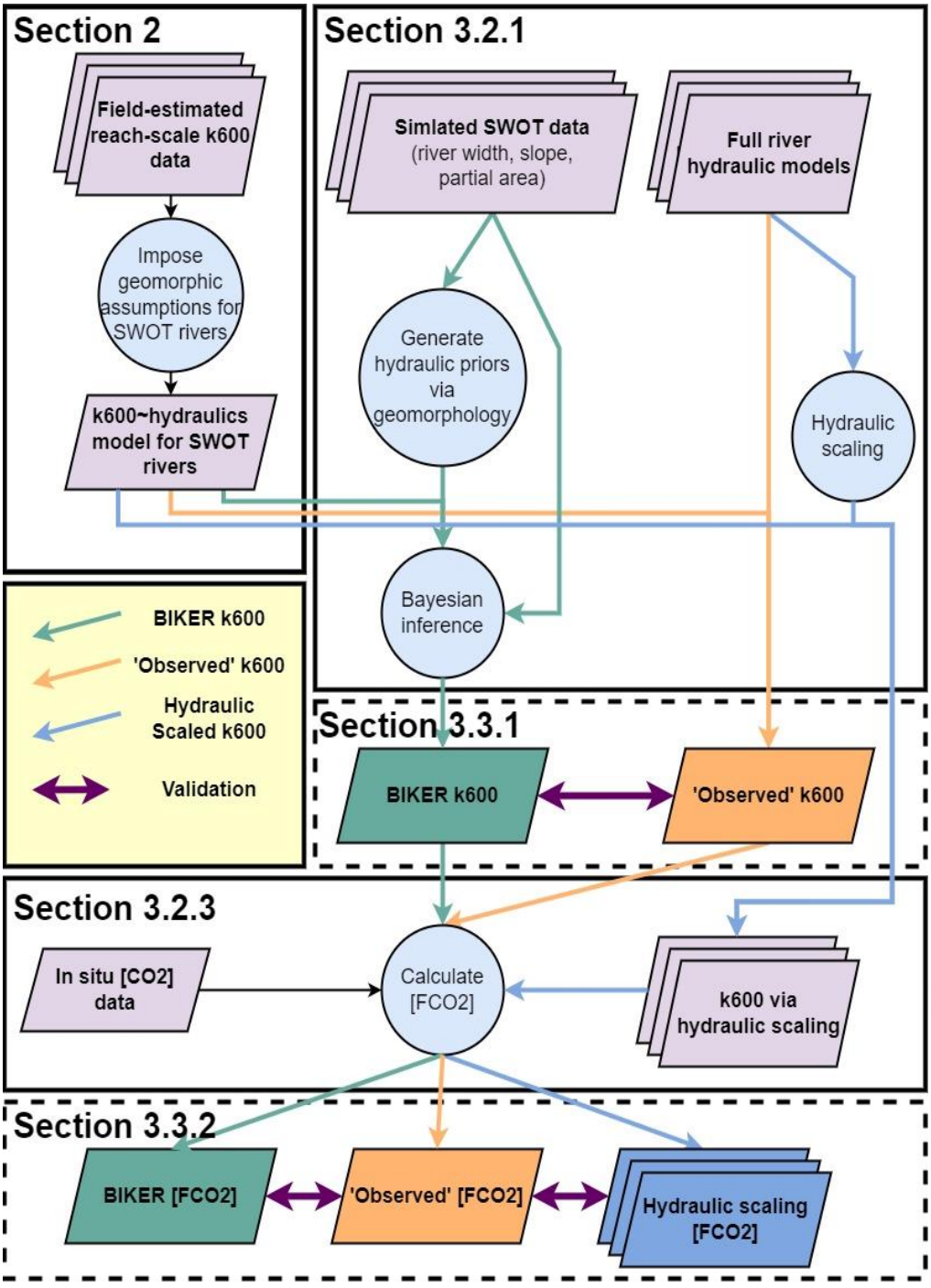

Figure S1: Flowchart detailing entire study workflow.

Figure S2

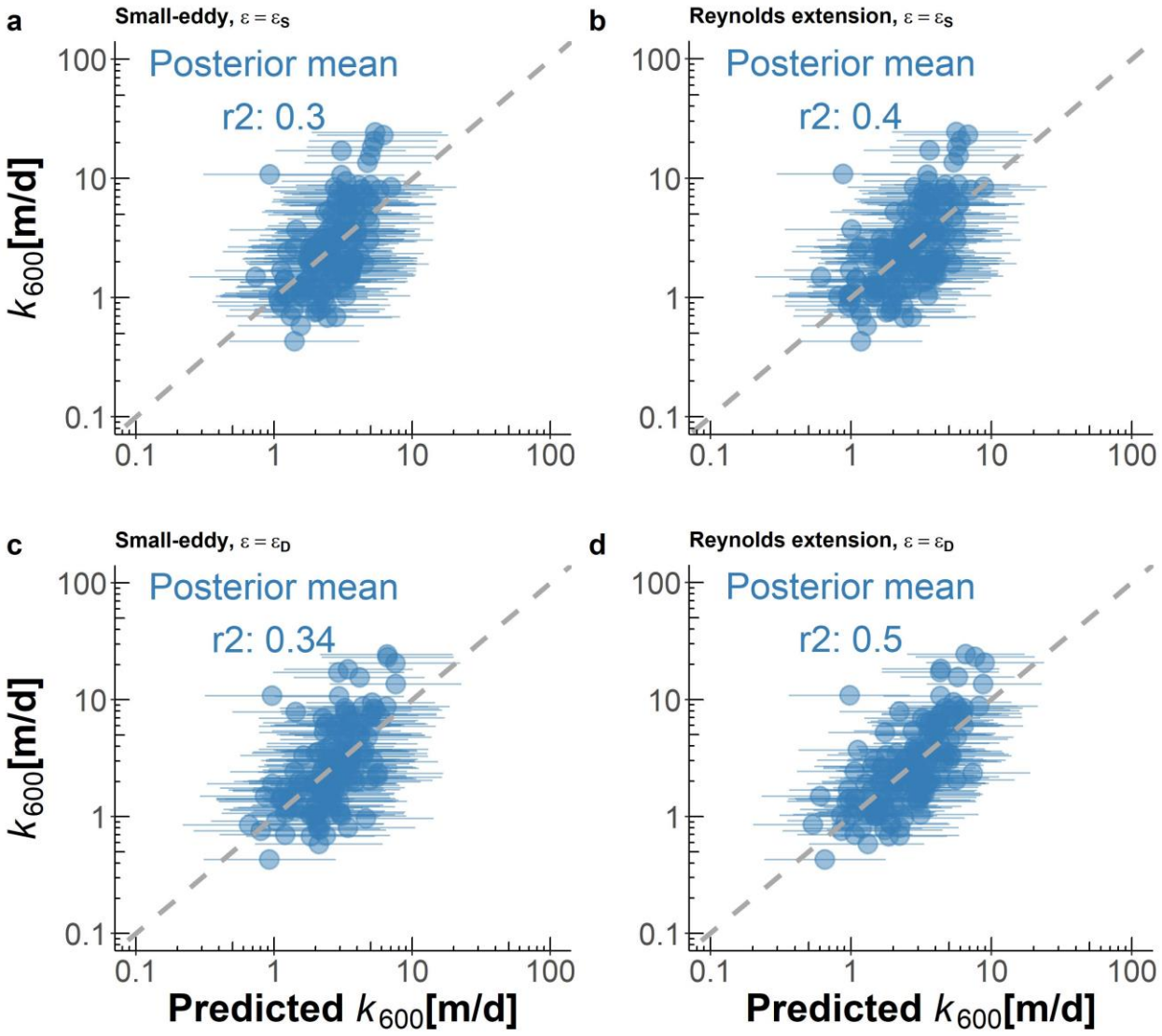

Figure S2: Four k_{600}~hydraulics models tested in this study, with model assumptions noted in the sub-panel titles. Panel (d) is also presented in the main text as Figure 2 and Equation 8.

Figure S3

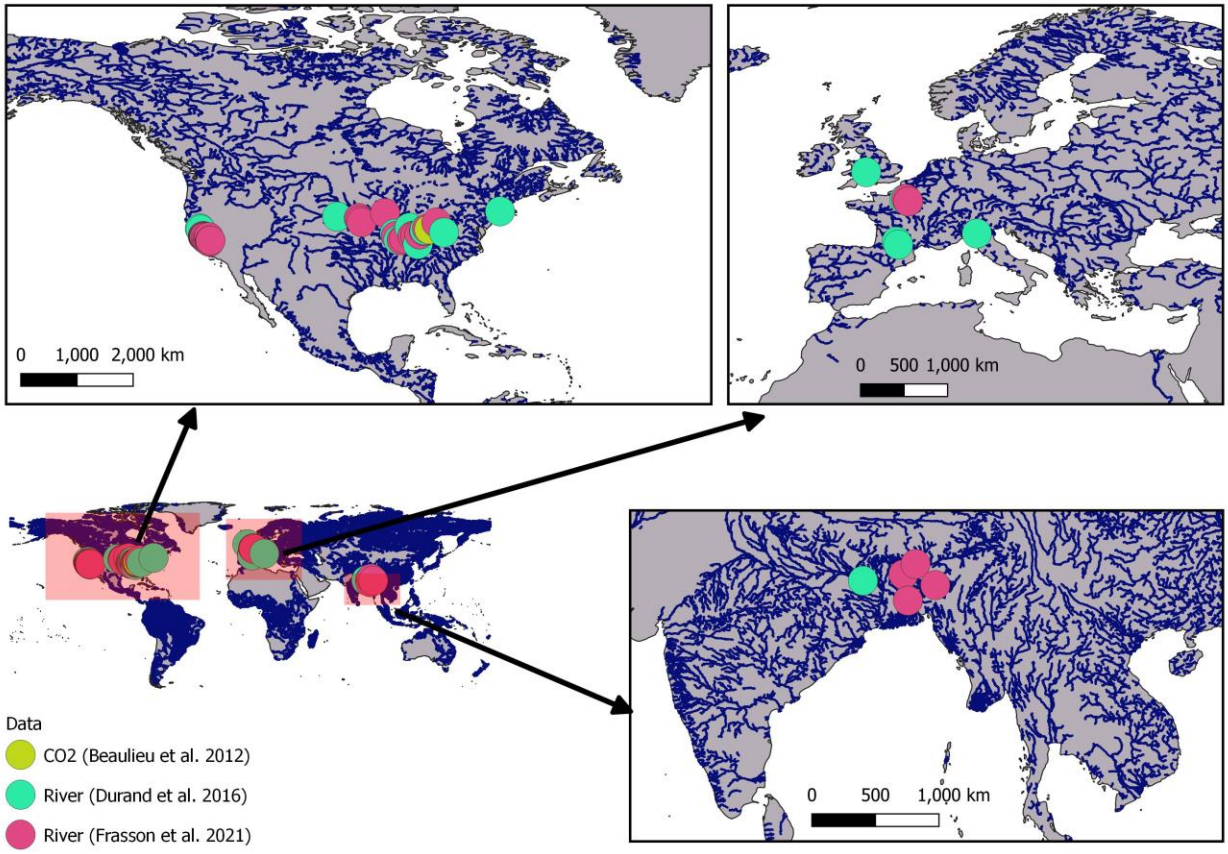

Figure S3: Map of simulated SWOT river locations along the global SWOT river network (Altenau et al., 2021). This corresponds to every river that BIKER could be run on once SWOT launches. Also includes approximate location of the $[CO_2]$ timeseries used in this study (Figure S4). Note that river locations are approximate as some hydraulic models are not geo-referenced.

Figure S4

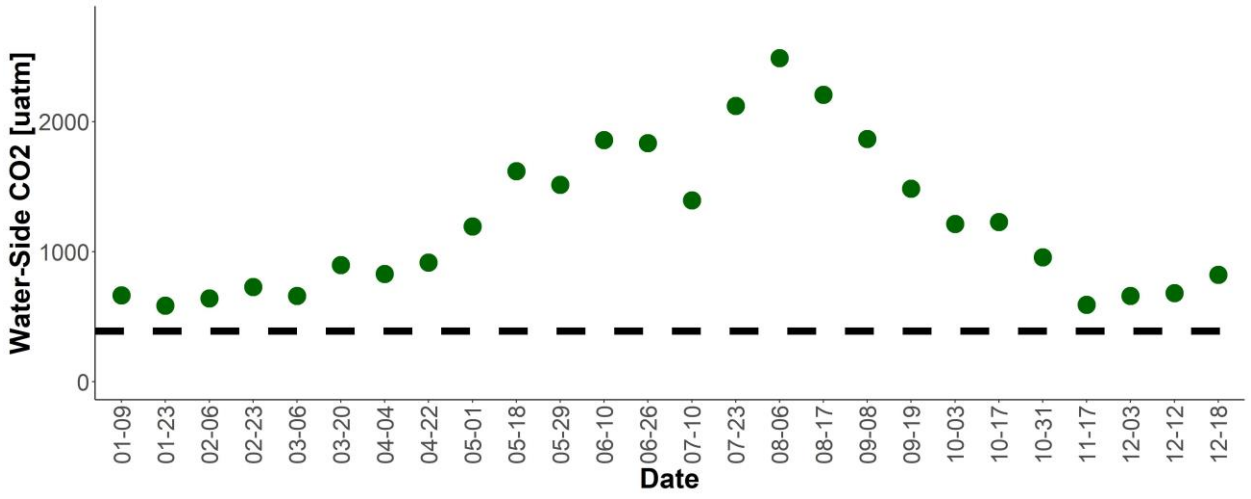

Figure S4 Timeseries of the biweekly $[CO_2]$ *data from Beaulieu et al. (2012). Sampling took place 2008-2009 in the Ohio River (upstream of Cincinnati, Ohio, United States). Dashed black line denotes atmospheric* $[CO_2]$ *at 400 uatm.*

Figure S5

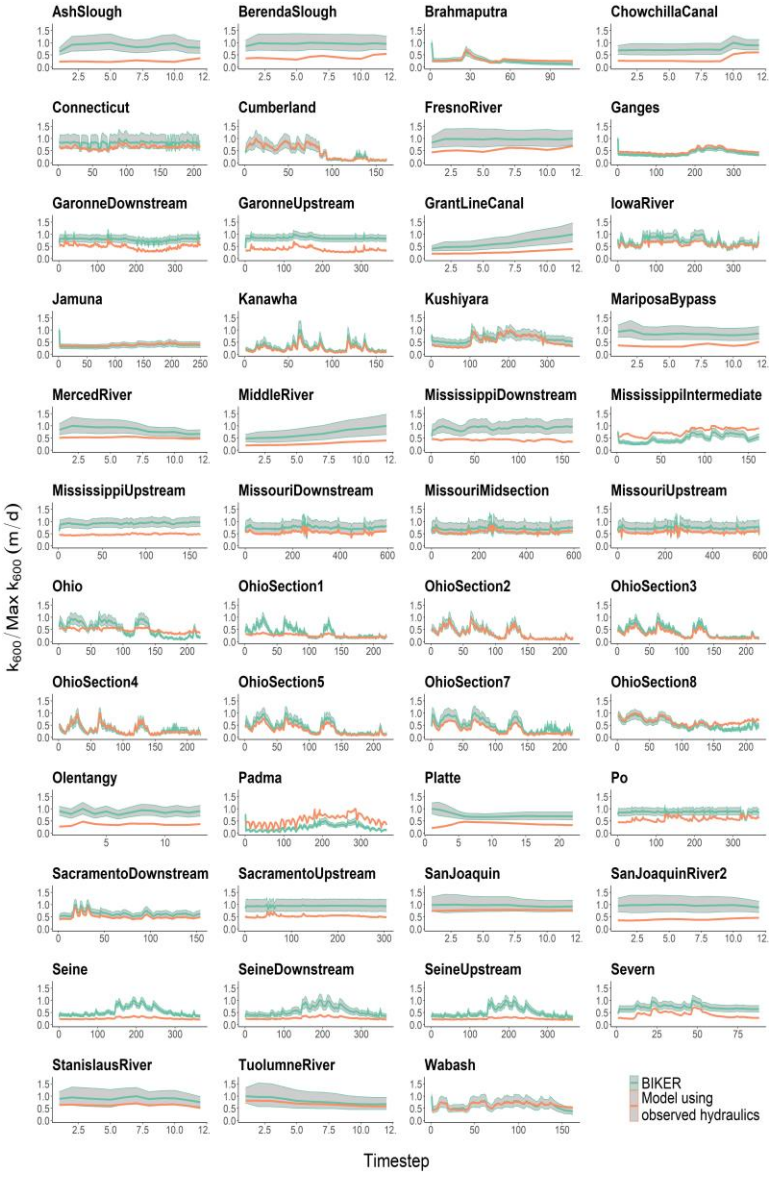

Figure S5: Observed (orange) versus BIKER-inferred (green) timeseries of daily k_{600} for the 47 SWOT-simulated rivers under the 'no-measurement-error' scenario. Green ribbon is BIKER posterior 95% credible intervals. Note that the y axis is normalized by maximum observed values to compare across rivers.

Figure S6

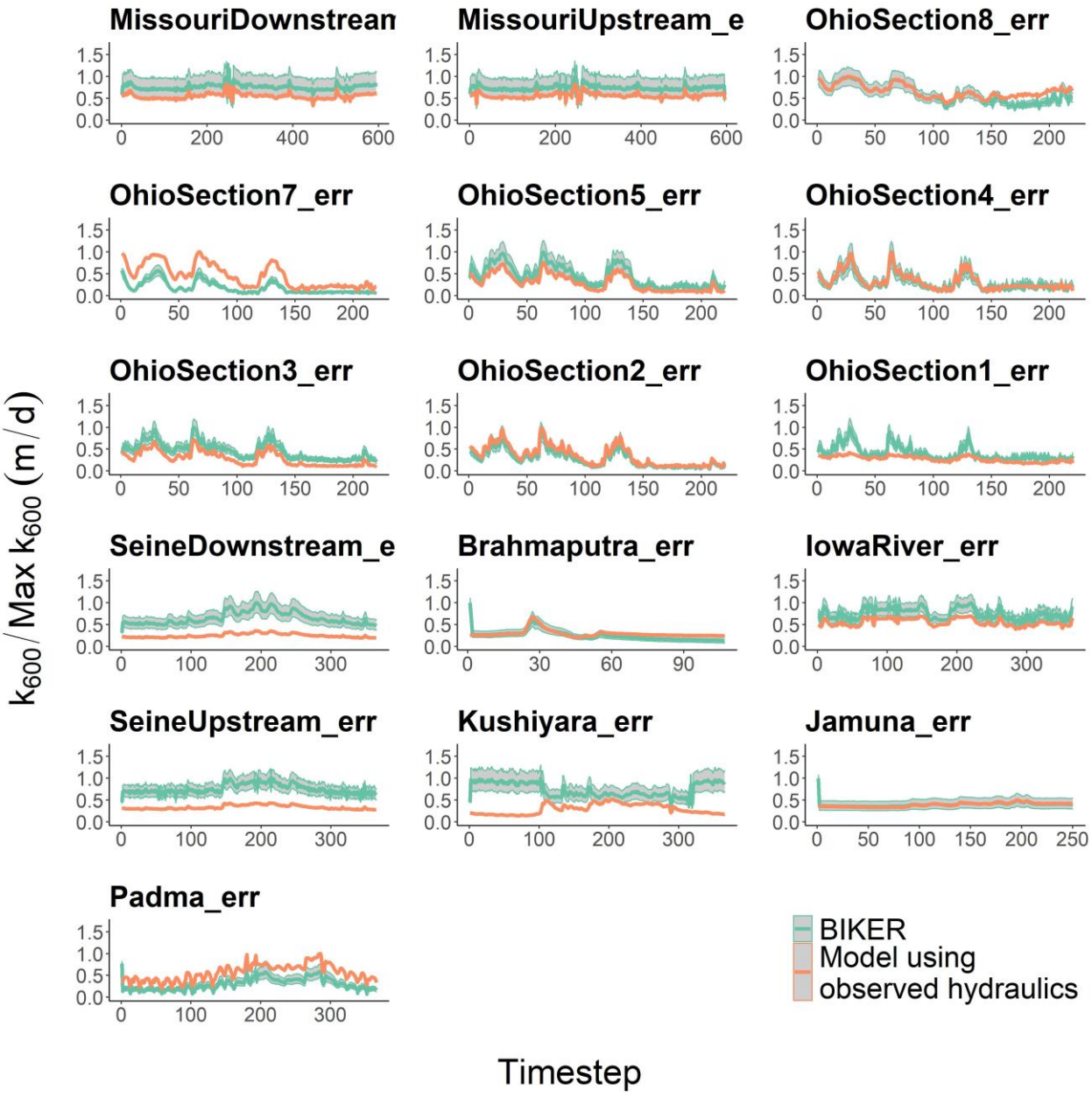

Figure S6: Observed (orange) versus BIKER-inferred (green) timeseries of daily k_{600} for 16 rivers under the 'measurement-error' scenario. Green ribbon is BIKER posterior 95% credible intervals. Note that the y axis is normalized by maximum observed values to compare across rivers.

Table S1

Table S1: Studies that gas exchange velocity measurements come from. 'Study' refers to the paper from which these measurements were obtained by us. Any data wrangling was done by those authors. 'Workers' refers to who actually made the measurements in the field. The Raymond et al. (2012) dataset is itself a meta-analysis. Please see that paper for how those measurements were collected, and see the 'Additional Studies' for the workers who actually collected the measurements.

Study	**Workers**	**Additional studies**
Ulseth et al. (2019)	Ulseth et al. (2019)	NA
Ulseth et al. (2019)	Hall & Madinger (2018)	NA
Ulseth et al. (2019)	Schelker et al. (2016)	NA
Ulseth et al. (2019)	Maurice et al. (2017)	NA
Ulseth et al. (2019)	Raymond et al. (2012)	Melching & Flores (1999); Bott, Montgomery, et al. (2006); Bott, Newbold, et al. (2006); Mulholland et al. (2001); Bernot et al. (2010); Tsivoglou & Wallace (1972)
Churchill et al. (1964)	Churchill et al. (1964)	NA
Owens et al. (1964)	Owens et al. (1964)	NA

Table S2

Table S2: Validation metrics used in this study, where Nt is number of observations and i is the specific observation. σ refers to the variance of the sample and μ refers to the mean of the sample. Carrot accents indicate the predicted value.

Description	Acronym	Definition	Ideal Score	Possible Range
Correlation Coefficient	r	$\sqrt{1-\left(\frac{\sum_{i=1}^{N_t}\left(k_{600,i}-\widehat{k_{600_i}}\right)^2}{\sum\left(k_{600,i}-\mu_{k_{600}}\right)^2}\right)}$	1	-1 to 1
Normalized root-mean-square error	NRMSE	$\sqrt{\frac{1}{N_t}\sum_{i=1}^{N_t}\left(\frac{\widehat{k_{600,i}}-k_{600,i}}{\mu_{k_{600,i}}}\right)^2}$	0	0 to ∞
Kling-Gupta Efficiency	KGE	$1-\sqrt{\left(r\left(k_{600_i},\widehat{k_{600_i}}\right)-1\right)^2+\left(\frac{\mu_{\widehat{k_{600}}}}{\mu_{k_{600}}}-1\right)^2+\left(\frac{\sigma_{\widehat{k_{600}}}/\mu_{\widehat{k_{600}}}}{\sigma_{k_{600}}/\mu_{k_{600}}}-\right.}$	1	-∞ to 1
Normalized Mean Absolute Error	MAE	$\frac{\frac{\sum_{i=1}^{N_t}\left(\left\lvert\widehat{k_{600_i}}-k_{600_i}\right\rvert\right)}{n})}{\mu_{k_{600}}}$	0	0 to ∞

Table S3

Table S3: Details on the 3 literature models for CO_2 fluxes. See Text S6 for more details.

Name	Depth equation	Velocity equation	Description	Reference
Brinkerhoff 2019	$D = 0.252Q^{0.388}$	$\bar{U} = 0.276Q^{0.164}$	104,624 measurements made across the United States at streamgauges	Brinkerhoff et al. (2019)
Raymond 2012	$D = 0.409Q^{0.294}$	$\bar{U} = 0.194Q^{0.285}$	1,026 measurements across the United States	Raymond et al. (2012)
Raymond 2013	$D = 0.409Q^{0.294}, D = 0.449Q^{0.37}$	$\bar{U} = 0.194Q^{0.285}, \bar{U} = 0.346Q^{0.120}$	Average of the Raymond 2012 equation and one using 9,811 measurements at US streamgauges	Raymond et al. (2013)

Table S4

Table S4: Comparison of SWOT-observable hydrography and global hydrography (at mean annual streamflow conditions).

Hydrography Model	**Surface Area [km^2]**	**Length [km]**
SWOT River Network (Altenau et al., 2021)	343,483	1,417,667
Most recent global hydrography estimate (Liu et al., 2022)	811,000	443,509,286
% that SWOT observes [%]	42.4%	0.3%

References

Altenau, E. H., Pavelsky, T. M., Durand, M. T., Yang, X., Frasson, R. P. de M., & Bendezu, L. (2021). The Surface Water and Ocean Topography (SWOT) Mission River Database (SWORD): A Global River Network for Satellite Data Products. *Water Resources Research*, *57*(7), e2021WR030054. https://doi.org/10.1029/2021WR030054

Beaulieu, J. J., Shuster, W. D., & Rebholz, J. A. (2012). Controls on gas transfer velocities in a large river. *Journal of Geophysical Research: Biogeosciences*, *117*(G2). https://doi.org/10.1029/2011JG001794

Bernot, M. J., Sobota, D. J., Hall Jr, R. O., Mulholland, P. J., Dodds, W. K., Webster, J. R., et al. (2010). Inter-regional comparison of land-use effects on stream metabolism. *Freshwater Biology*, *55*(9), 1874–1890. https://doi.org/10.1111/j.1365-2427.2010.02422.x

Bott, T. L., Newbold, J. D., & Arscott, D. B. (2006). Ecosystem Metabolism in Piedmont Streams: Reach Geomorphology Modulates the Influence of Riparian Vegetation. *Ecosystems*, *9*(3), 398–421. https://doi.org/10.1007/s10021-005-0086-6

Bott, T. L., Montgomery, D. S., Newbold, J. D., Arscott, D. B., Dow, C. L., Aufdenkampe, A. K., et al. (2006). Ecosystem metabolism in streams of the Catskill Mountains (Delaware and Hudson River watersheds) and Lower Hudson Valley. *Journal of the North American Benthological Society*, *25*(4), 1018–1044. https://doi.org/10.1899/0887-3593(2006)025[1018:EMISOT]2.0.CO;2

Brinkerhoff, C. B., Gleason, C. J., & Ostendorf, D. W. (2019). Reconciling at-a-Station and at-Many-Stations Hydraulic Geometry Through River-Wide Geomorphology. *Geophysical Research Letters*, *46*(16), 9637–9647. https://doi.org/10.1029/2019GL084529

Brinkerhoff, C. B., Gleason, C. J., Feng, D., & Lin, P. (2020). Constraining Remote River Discharge Estimation Using Reach-Scale Geomorphology. *Water Resources Research*, *56*(11), e2020WR027949. https://doi.org/https://doi.org/10.1029/2020WR027949

Churchill, M. A., Elmore, H. L., & Buckingham, R. A. (1964). The Prediction of Stream Reaeration Rates. In B. A. Southgate (Ed.), *Advances in Water Pollution Research* (pp. 89–136). Pergamon. https://doi.org/10.1016/B978-1-4832-8391-3.50015-4

Durand, M. T., Gleason, C. J., Garambois, P. A., Bjerklie, D., Smith, L. C., Roux, H., et al. (2016). An intercomparison of remote sensing river discharge estimation algorithms from measurements of river height, width, and slope. *Water Resources Research*, *52*(6), 4527–4549. https://doi.org/10.1002/2015WR018434

Frasson, R. P. de M., Durand, M. T., Larnier, K., Gleason, C., Andreadis, K. M., Hagemann, M., et al. (2021). Exploring the factors controlling the error characteristics of the Surface Water and Ocean Topography mission discharge estimates. *Water Resources Research*, *n/a*(n/a), e2020WR028519. https://doi.org/https://doi.org/10.1029/2020WR028519

Hagemann, M. W., Gleason, C. J., & Durand, M. T. (2017). BAM: Bayesian AMHG-Manning Inference of Discharge Using Remotely Sensed Stream Width, Slope, and Height. *Water Resources Research*, *53*(11), 9692–9707. https://doi.org/10.1002/2017WR021626

Hall, R. O., & Madinger, H. L. (2018). Use of argon to measure gas exchange in turbulent mountain streams. *Biogeosciences*, *15*(10), 3085–3092. https://doi.org/10.5194/bg-15-3085-2018

Hoff, P. D. (2009). *A First Course in Bayesian Statistical Methods*. New York: Springer.

Liu, S., Kuhn, C., Amatulli, G., Aho, K., Butman, D. E., Allen, G. H., et al. (2022). The importance of hydrology in routing terrestrial carbon to the atmosphere via global streams and rivers. *Proceedings of the National Academy of Sciences*, *119*(11), e2106322119. https://doi.org/10.1073/pnas.2106322119

Maurice, L., Rawlins, B. G., Farr, G., Bell, R., & Gooddy, D. C. (2017). The influence of flow and bed slope on gas transfer in steep streams and their implications for evasion of CO2. *JOURNAL OF GEOPHYSICAL RESEARCH-BIOGEOSCIENCES*, *122*(11), 2862–2875. https://doi.org/10.1002/2017JG004045

Melching, C. S., & Flores, H. E. (1999). Reaeration Equations Derived from U.S. Geological Survey Database. *Journal of Environmental Engineering*, *125*(5), 407–414. https://doi.org/10.1061/(ASCE)0733-9372(1999)125:5(407)

Mulholland, P. J., Fellows, C. S., Tank, J. L., Grimm, N. B., Webster, J. R., Hamilton, S. K., et al. (2001). Inter-biome comparison of factors controlling stream metabolism. *Freshwater Biology*, *46*(11), 1503–1517. https://doi.org/10.1046/j.1365-2427.2001.00773.x

Owens, M., Edwards, R. W., & Gibbs, J. W. (1964). Some reaeration studies in streams. *Inter. J. Air Water Poll.*, *8*, 469–486. Retrieved from https://ci.nii.ac.jp/naid/10025707421/

Raymond, P. A., Zappa, C. J., Butman, D., Bott, T. L., Potter, J., Mulholland, P., et al. (2012). Scaling the gas transfer velocity and hydraulic geometry in streams and small rivers. *Limnology and Oceanography*, 41–53. https://doi.org/10.1215/21573689-1597669@10.1002/(ISSN)1939-5590.MethaneVI

Raymond, P. A., Hartmann, J., Lauerwald, R., Sobek, S., McDonald, C., Hoover, M., et al. (2013). Global carbon dioxide emissions from inland waters. *Nature*, *503*(7476), 355–359. https://doi.org/10.1038/nature12760

Schelker, J., Singer, G. A., Ulseth, A. J., Hengsberger, S., & Battin, T. J. (2016). CO2 evasion from a steep, high gradient stream network: Importance of seasonal and diurnal variation in aquatic pCO2 and gas transfer. *Limnology and Oceanography*, *61*(5), 1826–1838. https://doi.org/https://doi.org/10.1002/lno.10339

Tsivoglou, E. C., & Wallace, J. R. (1972). *Characterization of Stream Reaeration Capacity*. U.S. Government Printing Office.

Ulseth, A. J., Hall, R. O., Boix Canadell, M., Madinger, H. L., Niayifar, A., & Battin, T. J. (2019). Distinct air–water gas exchange regimes in low- and high-energy streams. *Nature Geoscience*, *12*(4), 259–263. https://doi.org/10.1038/s41561-019-0324-8